AFSCET

Res-Systemica

Revue Française de Systémique

Fondée par Evelyne Andreewsky

Volume 20, printemps 2020

Modélisation systémique
de systèmes cyber-physiques

Res-Systemica, volume 20, article 07

Kilometric detection model of small, agile targets using a single emitter scanning lidar

Alain Quentel, Olivier Maurice, Xavier Savatier

19 pages

contribution reçue le 19 mars 2020

KILOMETRIC DETECTION MODEL OF SMALL, AGILE TARGETS USING A SINGLE EMITTER SCANNING LIDAR

A PREPRINT

Alain Quentel *
ArianeGroup - IRSEEM
Les Mureaux - St Etienne-du-Rouvray, France
alain.quentel@ariane.group
* corresponding author

Olivier Maurice
ArianeGroup
Les Mureaux, France
olivier.maurice@ariane.group

Xavier Savatier
IRSEEM
St Etienne-du-Rouvray, France
xavier.savatier@esigelec.fr

April 8, 2020

ABSTRACT

Remotely detecting and recognizing small, agile targets of interests at a kilometric range is a very complex task. Thanks to component maturation, laser-based systems can offer added values to other conventional systems such as radio-wave, radar, camera or even acoustic solutions. Taking the example of small, commercial drone detection, we first review the principles of LiDAR systems, and of other classic approaches. Then, we model the performances of a single emitter LiDAR imager across range, in terms of probability of detecting a given number of echoes on the target. Coupled to a numeric approach, our model can be applied to get an idea of the maximal range at which the system gathers enough target echoes for a classifying algorithm to accurately work.

1 Introduction

LiDAR systems are rich in phenomenology. Shortly after the invention of the laser, large scale experiments were already conducted to get distance measurement for atmospheric studies [1]. The field quickly expanded to aerosol and wind sensing [2], 3D topography [3], and structural vibrometry [4]. Hard target laser imagers, which is the application we will focus on in this paper, is currently getting more development and usage. This increasing popularity is directly linked to the recent need for more accurate, more resolved, cheaper and smaller 3D imagers for autonomous vehicles. The automotive mass market perspective has indeed been drawing component maturation and system development for the past few years [5].

The versatility, compact size, and potential kilometric range of LiDAR systems make them a potentially viable solution to detect and track small and agile targets. One interesting application is drone and UAVs (unmanned aerial vehicles) surveillance, which is quickly becoming a concern in sensitive areas such as airport, nuclear facilities, diplomatic buildings, etc... This is shown by the constantly increasing number of incidents [6].

We structure this paper in the following way. At first, we give an overview of the principles and technologies used in LiDAR system. Then, we extend to the subject of remote UAV detection and tracking, reviewing multiple systems based on electro-opto-acoustic solutions. At last, we model the performances of our single emitter scanning LiDAR in the purpose of providing enough detection points to classify small, agile targets at long range.

2 LiDAR main concepts and designs

Throughout LiDAR developments, researchers and engineers have sought to apply methods and processes that were already used in radio wave applications (radar), as both techniques use an electromagnetic wave emitter and receptor. Independently of its detailed structure, a LiDAR is composed of a single or plural laser emitter, a single or plural photodetectors and an optical emitting and receiving aperture. Once emitted, the laser light travels through the medium, usually the atmosphere, before reaching the scene to image. The light then scatters on the objects, and a portion travels back to the receiving aperture. It is this portion of light that must be processed to extract the range information.

This introduction is meant to give a brief descriptions of the principles and technologies used in LiDAR system. More details can be found on various books [7, 8] and articles [9, 10, 11].

2.1 Accessing range

Light is a wave that, when emitted, propagates through a medium. Because the wave travels at the speed of light, the wave instantaneous module and phase acquire an offset. The light amplitude A can be written in the form

$$A[t] = M[t - \frac{x}{c}] \exp(i\omega(t - \frac{x}{c}) + \phi[t - \frac{x}{c}]) \,, \tag{1}$$

with t representing time, ω the center frequency and x the traveled distance. The module M and the phase ϕ are here written as functions of time, as they can potentially be modulated. Range information is also contained in the frequency term, but because the light wavelength is in the order of a micro-meter or less, the 2π ambiguity makes it unusable for most applications. Therefore it is dropped in the following equations of this paper. With the wave equation detailed, we can review the different ways to access the range information.

2.1.1 Frequency Modulation

This method, which is the most complex, relies on light coherence. Most LiDAR systems employing this method for hard target detection use frequency modulated continuous wave (FMCW). The main principle is to chirp the laser optical frequency across time, using for instance a triangular frequency modulation. When the wave propagates in the medium, it acquires a phase delay proportional to the traveled distance. Because of the very high frequency of visible or infrared light (terahertz band), working with the full waveform in the electronic domain like what is done with radar is impossible. Therefore, one need to use the coherence property of laser light to create an optical interference pattern on the detector by superposing the reference wave (called the local oscillator, lo) with the backscattered one, ba. This process acts as a frequency subtraction between the waves, lowering the center frequency. The coherent light amplitude subtraction produces on the photodetector a light intensity I of expression

$$I[t] = |M_{lo} \exp(i\omega t + \phi[t]) + M_{ba} \exp(i\omega t + \phi[t - \frac{x}{c}]t)|^2 \,, \tag{2}$$

$$= M_{lo}^2 + M_{ba}^2 + 2M_{lo}M_{ba} \cos((\phi[t - \frac{x}{c}] - \phi[t])t) \,. \tag{3}$$

If the frequency modulation used is a triangle wave of period T and peak-to-peak amplitude B, then on the up-ramp, we have

$$\phi[t] = \frac{2B}{T} t \,. \tag{4}$$

If the system points at a single static target at a distance $R = x/2$, then the obtained electrical signal after optical interference contain a single intermediate frequency (IF) f_{if} of value $f_{if} = 4RB/(cT)$. If the target is moving, the frequency content of the backscattered wave is shifted due to the Doppler effect. This shift can be uncoupled from the distance in the IF by analyzing the behavior in the up-ramp compared to the down-ramp [12]. The range is then given by

$$R = \left(\frac{f_+ + f_-}{2} \right) \frac{cT}{4B} \,, \tag{5}$$

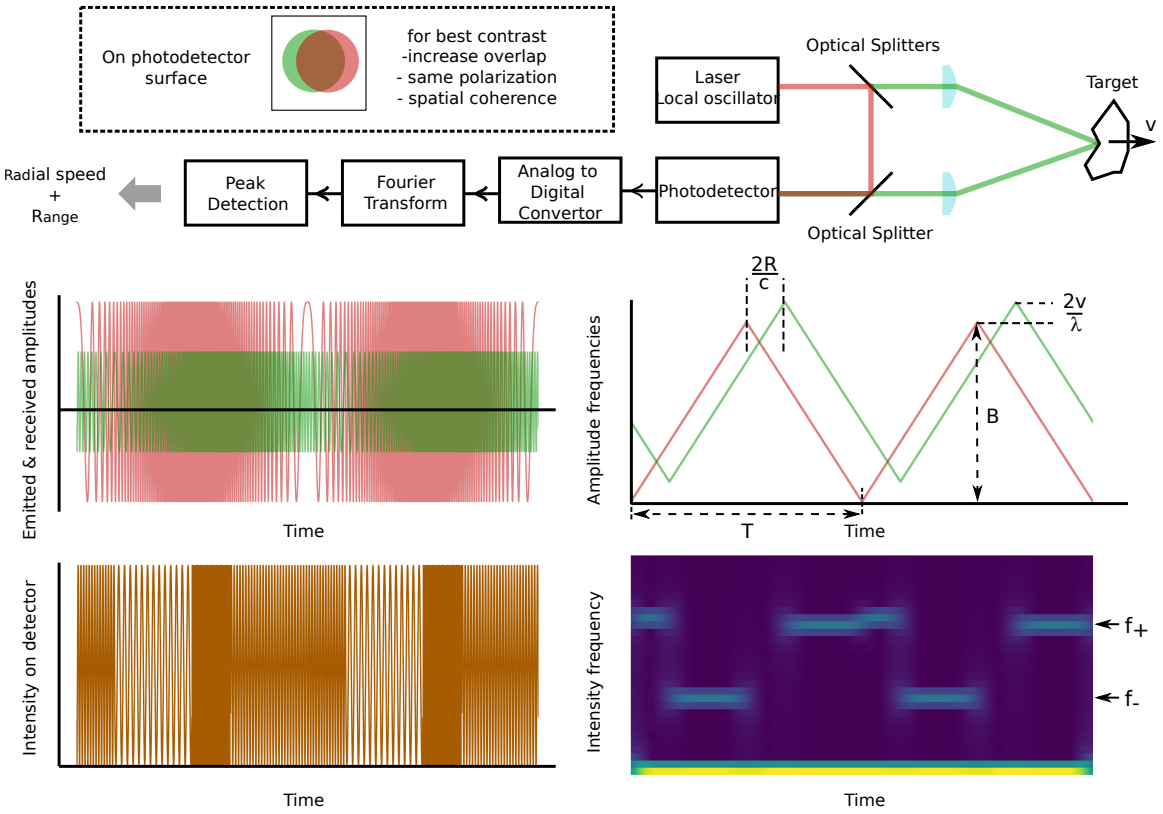

Figure 1: (Up) schematic of a FMCW LiDAR. (Down, up left) emitted (red) and received (green) light amplitude as a function of time for a distant moving target. (Down, up right) frequency content as a function of time for both amplitudes. (Down, down left) light intensity of the photodetector as a function of time, showing interference pattern. (Down, down right) sliding Fourier transform of the intensity, showing the frequency content as a function of time.

and the target radial speed is

$$v = \left(\frac{f_+ - f_-}{2} \right) \frac{\lambda}{2} , \tag{6}$$

with λ the laser wavelength. Therefore, a well designed FMCW LiDAR provides both range and speed information, at least in the illumination direction. These considerations are illustrated on Fig. 1.

Because of the speed information, FMCW LiDAR is a very interesting option. Moreover, it is based on light coherence, thus rejecting all other light sources that does not comes from the laser itself, including solar background. Yet to maximize the signal that can be exploited, the two beams must overlap, with as little wavefront and polarization distortion as possible. The alignment is thus very critical. Moreover, the modulated waveform linearity is a key factor for good signal to noise (SNR) ratio [13]. Because it is an indirect measurement, an important amount of processing must be performed to gather distance and speed. This can be done in the analog or digital domain, using for the latter appropriate analog to digital converters (ADC) and fast Fourier transform (FFT) algorithms.

The laser line-width (the frequency spread of the optical wave frequency content) limits the maximum accessible range. After this distance, the return frequency gets too broaden and sink into noise. A kilometer range would for instance require a 100 kHz linewidth, which may be difficult to get across with compact laser diodes. Advanced signal processing can be used to improve detection at long range [14], but the fundamental limits remains. The source stability is also impacted by other factors such as temperature and usage wear. Due to those strong requirements in linearity and line-width, limitations in average power for commercial products can inherently limits the maximum range. Because of these constraints and the overall complexity, FMCW was not the retained solution for the system presented in this paper.

Finally, for wind sensing, pulsed - rather than continuous - coherent sources are used, with relatively long (a few hundreds of nanoseconds) pulse length. Using pulses instead of continuous waves yield poorer range resolution due to large pulse width, but allows for better decoupling between velocity and range. The higher peak power also allows for higher range while keeping an "eye-safe" low average power, at the expense of a bulkier architecture [15].

2.1.2 Intensity Modulation

The other option is to modulate the module of the light wave. For this method, incoherent detection - or energy detection, is used. As explained before, the frequency of light is too high to be directly acquired by any electronics, and therefore photodetectors can only access the intensity envelope. To use a radio-wave analogy, the lightwave acts as a carrier frequency for intensity modulation distance measurement.

amplitude-modulated continuous wave (AMCW) In amplitude-modulated continuous wave (AMCW) LiDAR, the intensity is modulated using a periodic signal. We wish to present here a way to extract range using direct signal multiplication and filtering, such as in [16]. Yet some commercial systems employ signal digitization to perform correlation between the reference and the back-scattered light intensity, using either cross-correlation or Fourier transform multiplication [17]. Here we presents a "lock-in" type of detection. One need to take the product between the reference and the back-scattered light intensity, giving:

$$\begin{aligned} X[t] = &\ |M[t-\frac{x}{c}]\text{exp}(i\omega t+\phi)|^2\ |M[t]\text{exp}(i\omega t+\phi)|^2\ , &(7)\\ = &\ M[t-\frac{x}{c}]^2\ M[t]^2\ , &(8)\\ = &\ I[t-\frac{x}{c}]\ I[t]\ . &(9)\end{aligned}$$

If the modulation is sinusoidal, then

$$I[t] = B\text{cos}(\omega_m t)\ , \tag{10}$$

with ω_m the modulation angular frequency and B its amplitude. The direct and quadratic product X and Y can then be written as

$$X[t] = \frac{B^2}{2}(\text{cos}(2\omega_m t-\frac{x}{c})+\text{cos}(\omega_m\frac{x}{c}))\ , \tag{11}$$

$$Y[t] = \frac{B^2}{2}(\text{sin}(2\omega_m t-\frac{x}{c})+\text{sin}(\omega_m\frac{x}{c}))\ . \tag{12}$$

By using low-pass filtering and computing $\Omega = \text{arctan}(Y_{filt}/X_{filt})$, one has access to $x = 2R$. In most systems, to get a more accurate range, the algorithm (lock-in type or cross-correlation) is usually performed at 4 four different phase shifts. Increasing ω_m directly increases the range resolution, but at the same time shortens the unambiguous range, i.e. the range at which a 2π period of the modulation is reached. For instance a 10 MHz modulation correspond to a maximum distance of a few tens of meters. Getting range with enough accuracy requires multiple waveform periods, which directly increases the time needed for each point.

Moreover, eye-safety legislation restricts the value of the laser light average power that can be emitted. Because of the direct intensity detection, sensitivity is directly proportional to the power amplitude of the laser source, and inversely proportional to the noise floor of the detection chain. Because of these aforementioned arguments, commercial applications are limited to very short distances, usually ten meters, or the size of a room. Time of flight (ToF) silicium cameras are usually used, coupled with near-infrared LED rather than lasers [9].

Pulsed ToF The second, most common form of intensity modulation is very certainly the pulsed ToF LiDAR. In this method, the laser emits a very short laser pulse. By acquiring the time difference between the emitted and received pulse, it is possible to perform a direct distance measurement with $R = c/(2\ \text{ToF})$. Usually, to get as much peak power as possible while keeping a reasonable photodetector bandwidth, pulse duration is in the nanosecond range [10]. Compared to AMCW, the narrow pulses allows for high peak power while keeping a low average power, therefore keeping up with the eye-safety limit.

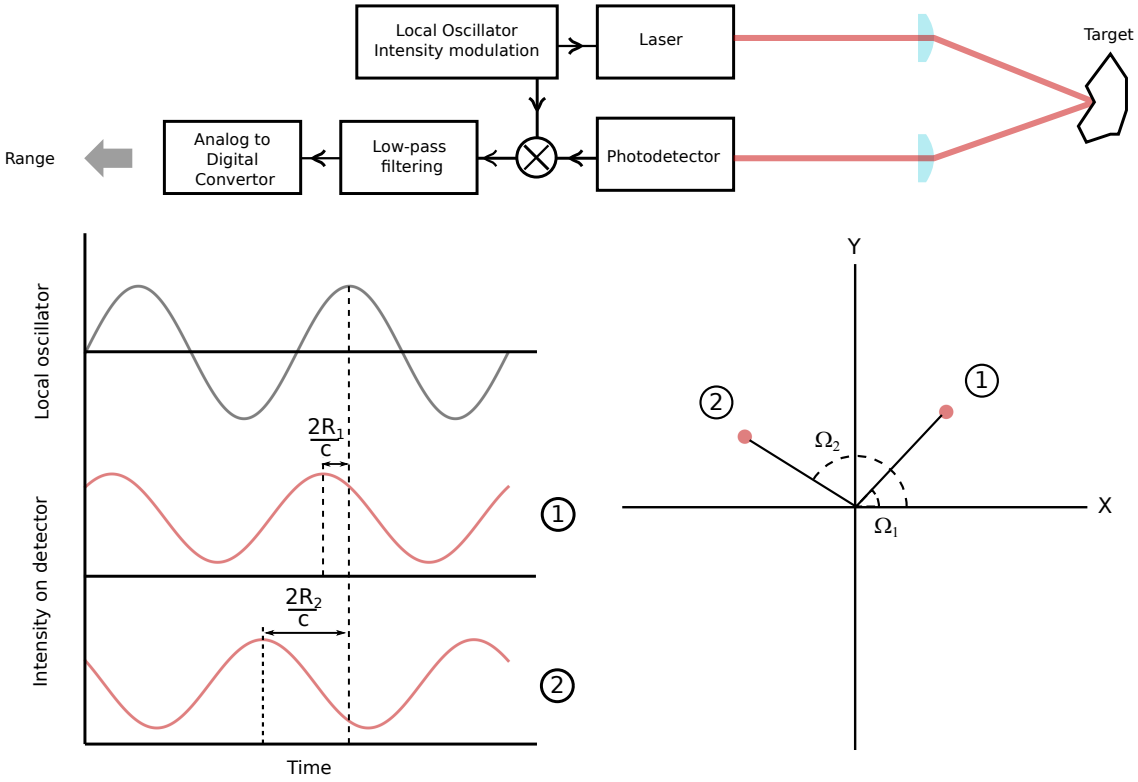

Figure 2: (Up) schematic of an AMCW LiDAR. (Down, left) local oscillator (black) and received (red) light intensity as a function of time, for two different ranges R_1 and R_2. (Down, right) XY plane representation of the filtered product. R_1 and R_2 can be deducted from the respective value of Ω_1 and Ω_2.

Pulse time-stamping can be done by processing the digitized return waveform, yet this approach requires a very high sampling rate digitizer and heavy data computation for real time application. Most systems uses fast analog triggering electronics [18]. Compared to the FMCW, the technique is sensitive to other light sources, most importantly the solar background. The use of a narrow bandpass optical filter can help mitigate its impact. Moreover, range accuracy is not a function of the modulation bandwidth like with FMCW, but is limited by rising edge or pulse centroïd detection precision, adding to jitters within the electronics. Changes in amplitude, or pulse broadening can therefore create pulse walk [19], which needs to be compensated. For those reasons, the overall ranging performance is usually in the centimeter range at best. Schematic of a pulsed LiDAR is presented on Fig. 3.

Because of its simplicity of implementation and long ranges performance, the pulse ToF LiDAR was the retained solution for our system.

2.2 Making a 3D image

Once we viewed the main options to retrieve distance, we can address the way LiDAR systems create a 3D image. There are three main types of LiDARs : staring, scanning, and hybrids. Each design possess its own advantages and drawbacks, but the core constraint is often the choice of detector, which limits either the field of view (FoV) or the resolution. Therefore, we choose here to present the section based on the detector type.

2.2.1 2D detector array

The detector can be comprised of a 2D array of pixels, working just like a camera, except it can perform range measurements. For FMCW and AMCW, the illumination is continuous. For pulse ToF, the illumination is pulsed, and the resulting system is called a flash LiDAR. In flash systems, the whole scene can be theoretically acquired in a single nanosecond flash, providing high refresh rates and a "frozen" image of the scene. Independently of the range method

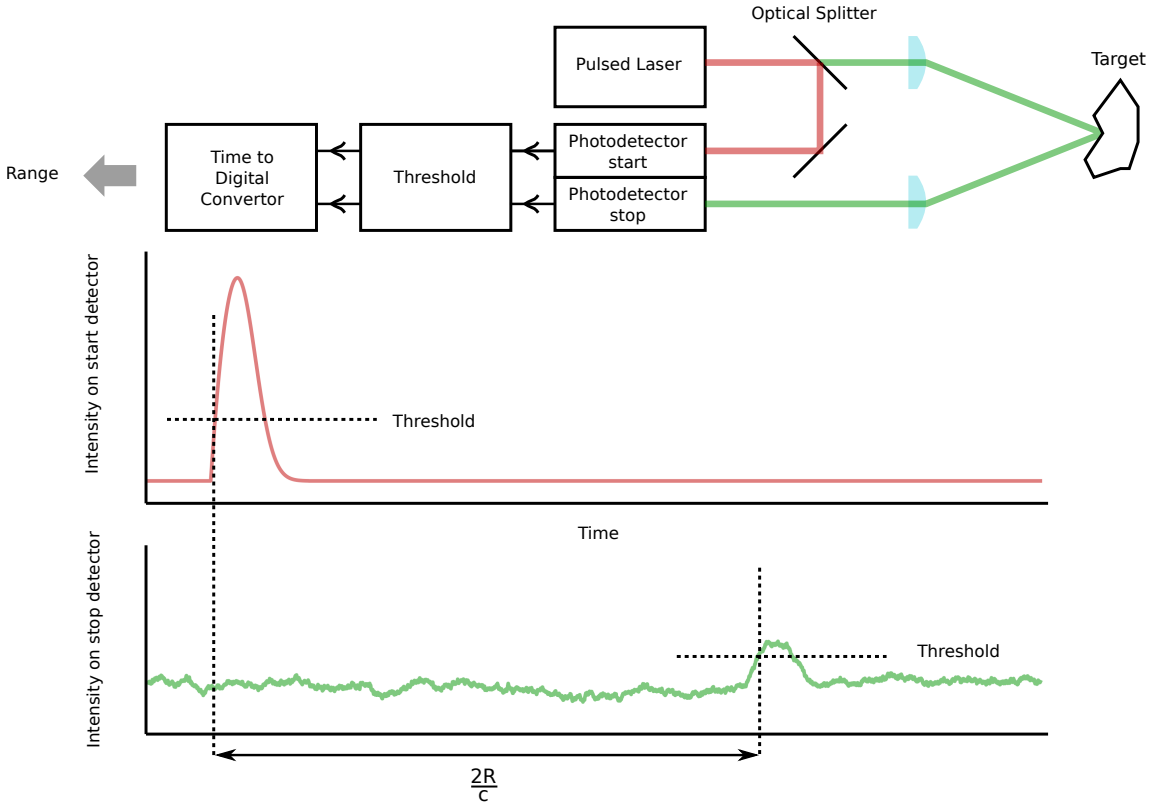

Figure 3: (Up) schematic of a pulsed LiDAR. (Down) emitted (red) and received noisy (green) light intensity as a function of time. Thresholding and time-flagging directly give access to target range.

used, the laser has to illuminates the FoV seen by the 2D array. Because of the loss in energy density, which squares with the FoV to cover, the maximum available range shortens very quickly. Moreover, the threshold for eye-safety also limits the laser power. An illustration of a flash LiDAR design is shown on Fig. 4.

The array pixel density and size brings its own limits regarding the compromise between FoV and resolution. In the NIR wavelength, around 900 nm, CCD or CMOS silicium based arrays are widely available at a low cost. They are mainly used for AMCW LiDAR, with specialized electronics to allow for light demodulation, such as the 320 x 240 pixels of [16]. The same type of detector could potentially be used for FMCW LiDAR, but processing the MHz intermediate beat frequency requires specialized electronics and signal processing functions that is very complex to implement on such a huge number of pixels. To the best knowledge of the authors, a full 2D array for FMCW LiDAR has not yet be realized with more than a few pixels. A workaround must be found to increase pixel resolution, like using an AMCW camera [20].

For pulsed flash LiDAR, the constraint is even higher, as a true ToF system with centimetric accuracy requires a high bandwidth photodetector and amplifier including a very high speed read out integrated circuit (ROIC). To increase the SNR, extremely sensitive arrays of detectors are usually used in this direct detection setup. In the NIR wavelength, which is the most widely used for current automotive LiDAR, silicium avalanche photodetector (APD) is the component of choice. Most arrays of detectors employ silicon photomultipliers (Si PM) [21], which are constituted of APD biased beyond their breakdown voltage, and are able to detect a single photon event. They are also called single photon avalanche detector, SPAD or Geiger-mode APD. With any single photo detector, there is a short time period (at the very minimum 100 ns) after each detection where the detector is blinded, called dead time. Moreoever, a phenomenom called after-pulses increases the false alarm rate right after this dead time, for a short period. Therefore, operation in a photon-rich environment such as daytime can be very challenging.

To alleviate eye-safety constraints for longer range system, it is possible to operate in the short-wave infrared (SWIR) band. At this wavelength, light does not penetrate cornea and therefore damage appears at higher power density. In

this waveband, commercially available arrays can be based on HgCdTe, which must be cooled, or on the more used InGaAs material. APD arrays on these materials are commercially available, reaching resolutions of 512x640 pixels [22]. Unfortunately, properly implementing ROIC able to time the nanosecond returning pulse is too complex to be done on such an important amount of pixels. To alleviate that constraint, these arrays are used for ToF application by applying an electronic shutter on the ROIC, so as to only accept light flux coming from a specific distance slice on the scene. Gate width is often in the tens of nanosecond order, which means a distance resolution of few tens of meters. Because these camera usually run at a few tens of hertz, varying the gate center image after image can be done to improve the range resolution of the image [23], while keeping refresh rate relatively high. Increasing range resolution has also been demonstrated using diverse compress sensing algorithms [24].

2.2.2 1D or quasi 1D linear detector array

With a 1D detector matrix, the laser light must illuminate a horizontal or vertical band of the scene, which is then swept across the orthogonal direction to produce the 2D image. Therefore, a beam steering component must be used. This setup is most often used for direct pulse detection, as the lower number of elements allows for implementation of high-bandwidth ROIC for real, direct pulse ToF measurements [25]. Such a setup also allows for increasing laser power density on the scene, as the instantaneous FoV will be smaller than for a 2D array. The loss in FoV must be compensated by the beam steerer, but scanning a single dimension may be acceptable and causes less wear than scanning in 2D [26]. Like previously mentioned, the technology is more mature, widespread and provides better performances in the NIR wavelength with silicium components than in the SWIR with InGaAs components.

Another solution commonly seen, most notably in Velodyne systems, is the use of one or more linear array of both laser emitters and receivers. Each laser is coupled to its single element photodetector in a vertical arrangement. The resulting system illuminates a vertical band, and is rotated in the horizontal direction to generate a 360° point cloud. The resolution on the other direction is given by the number of elements within the line FoV [27]. Outer LiDAR systems also employ this design, except that they are using microelectrico-mechanical systems (MEMS) mirrors instead, increasing compactness and lowering power consumption [28]. When electronically scanning a 2D detector array, the rows are addressed sequentially. Therefore a way lower number of ROIC and timing electronics is needed for accurate pulse detection. Such a method can be called quasi 1D. An illustration using a MEMS is shown on Fig. 4.

2.2.3 Single element photodetector

LiDAR comprising of single element photodetector are referred as purely scanning LiDAR. In this architecture, a narrow laser beam is continuously swept across the FoV. Each position of the beam scanner is stored to sequentially reconstruct the image. This method can provide both a long range, a wide FoV, and a high resolution depending on the scanner performances. 2D beam steering can be realized with a number of solutions such as mechanical galvanometers [29] or non-mechanical MEMS mirrors [30], rotating polygons [31] or prisms [32], and even solid-state photonics phase array [33]. Each one of these beam steerers can be clustered into different applications depending on their size, cost, mechanical bandwidth, laser power handling, access to position feedback and aperture.

Another advantage of scanning LiDAR is the component itself. Single element photodetectors are cheaper, usually more sensitive and more widely spread than arrays. Nevertheless, when considering a single source and single detector, flash LiDAR sensor will always have a far greater refresh rate at the equivalent FoV and resolution. Moreover, very intensive data processing may be required to analyze hundreds of thousands of 3D point clouds in real time, requiring advanced hardware and software. At last, designing a scanning LiDAR to meet given requirements in angular resolution, refresh rate, range and FoV is a complex problem, as most parameters critically depends on each other [34]. A monostatic scanning LiDAR implementation is shown on Fig. 4.

3 Related work

Multiples options has been consistently used for remote, automated detection and tracking of small, agile targets. To give a brief overview of what has been done, we will focus on drones or UAV (unmanned aerial vehicles). They indeed represent a challenging target in terms of size, speed and variability of behavior. Moreover, they can be operated in an urban or a more open environment, meaning that perception algorithms must work with very diverse backgrounds. Multiple acousto-electro-optical solutions have been developed to provide a solution to this problem, including LiDAR systems.

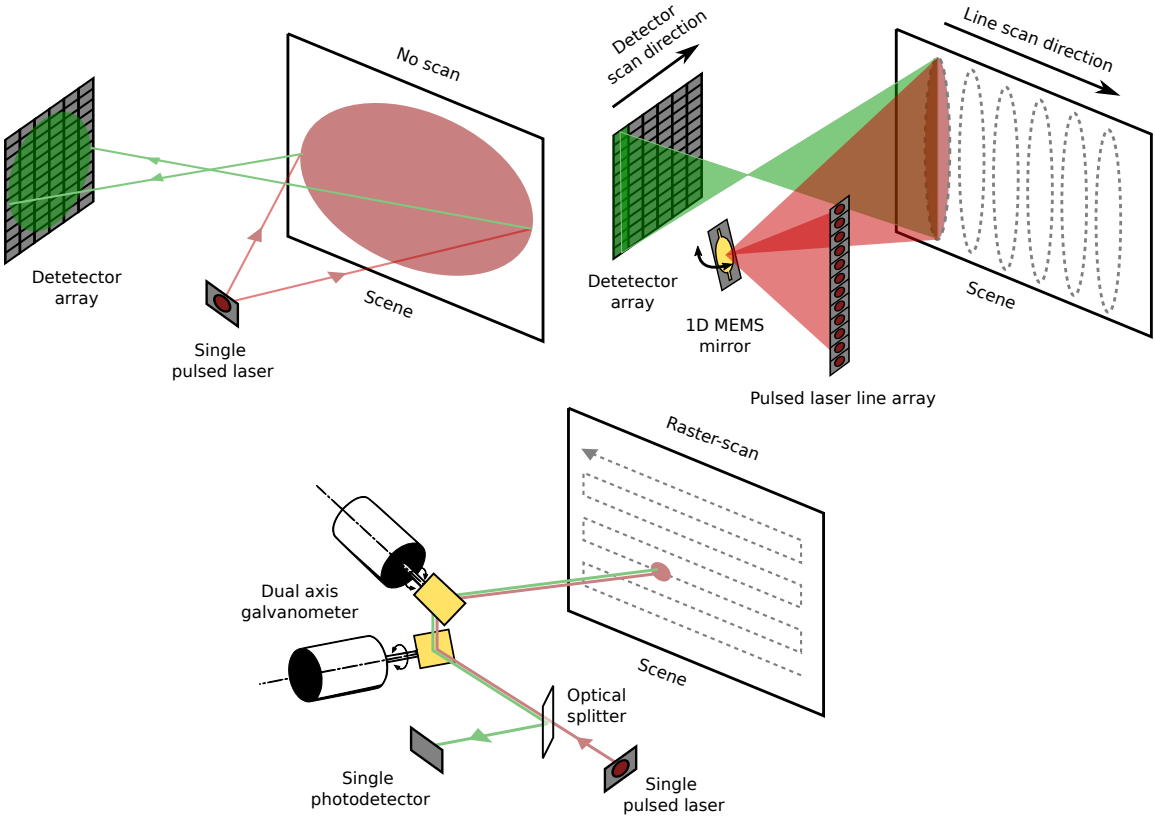

Figure 4: (Up, left) illustration of a flash LiDAR with a single pulsed emitter and a 2D detector array. (Up, right) illustration of a mixed-approach with a pulsed laser line array, a 1D MEMS mirror scanner and a synchronized electrically scanned 2D detector array. (Down) illustration of a 2D scanning LiDAR using two galvanometer mirrors. The configuration is monostratic with a single laser emitter and a single photodetector.

3.1 Not laser-based

This section describes the state of the art of UAV, drones, and more generally small, agile targets detection and tracking using systems other than laser-based. A selection of examples and systems is provided here, but more details can be found on the following articles [35, 36, 37, 38].

3.1.1 Passive radio-frequency and active RADAR

The radio-frequency (RF) domain extents from 3 kHz to 300 GHz. Amateur commercially available UAV are operated using a remote controller operating in the RF domain. By spying this link, it is possible to detect and track the UAV using a completely passive system. In the same waveband, an active radar emits and receives its own RF waves to detect and image the target. Inherently, a radar or a passive RF system has much less resolution than a LiDAR. Exactly like with a laser, the wave emitted or received by an antenna retains coherence properties. Diffraction theory shows that the beam divergence Θ can be given in order of magnitudes by:

$$\Theta = \frac{\lambda}{D} \,, \tag{13}$$

with λ the wavelength, and D the aperture. In the NIR, at a 1 μm wavelength, a laser of 1 cm of diameter at the exit of the system produces a beamwidth of 0.006°. This represents 10 cm at 1 km. With RF systems, the aperture is complex

to accurately compute. The beam divergence can instead be derived from the value of its directional gain G_i relative to an isotopic antenna by the approximate formula

$$\Theta = \sqrt{29000/G_i} \tag{14}$$

with Θ in degree. To give an order of magnitude, a 20 dBi antenna, such as the one used for RF drone detection in [39], produces a beamwidth of around 20°. This is the raw lateral resolution of the system, considerably lower than in the optical domain.

The advantage of the passive RF option is the relatively inexpensive components compared to the other solutions. Yet, non trivial line of sight and multipath propagation must be carefully studied to acquire the distance with a single receiver. Detection was experimentally demonstrated on distances of several hundred of meters [39]. The main difficulty resides in isolating the correct frequency band and channel and keeping tracks of potential hopping sequences on the carrier frequency [40]. Moreover, there are many types of hardware and software implementations across manufacturers and models. The control on older model can be analog, using a ten of MHz carrier frequency, or digital in newer model using classical Wifi band of 2.4 or 5.8 GHz, or even dual-band [41]. Adding to these the likely presence of other communications channels (from GSM, Wifi, radio, etc...) sinking the signal into noise, it is easy to see how challenging of an approach it is. Nevertheless, recognizing the drone model is possible if a data bank was previously built. Jamming the communication link once detected is also available with a correctly tuned emitter.

To improve accuracy and detection range, radar systems must be employed. Radar have very good penetration in bad weather (rain, fog, etc...), and can be operated during the night. By exploiting doppler effect like with the FMCW LiDAR, radar gets access to the instantaneous target speed. The main challenge that must be faced is the low radar cross-section of drones, and their low speed compared to usual radar targets. Drone discrimination against noise and clutter was shown to be improved by using micro-Doppler signatures in a multistatic configuration [42]. In [43], a 94 GHz radar (mm wave) was shown to produce a 15 cm range resolution, and was able to track target from 10 m up to several hundreds of meters. Finally, we can cite here experiments with DJI Phantom 2 and a radar prototype showing a maximum detection range of about 3 km [44].

Nevertheless, it should be stated that strong radar signals may not be suitable for a continuous urban use. Day long operation could potentially disrupt electro-sensitive equipment. Moreover, radar systems used in civil area should comply to exposure limits within the norm of the country [45], which could limit its accessible power and thus maximal range. These constraints are obviously shared with active LiDAR systems.

3.1.2 Acoustic sensor

When flying, drones produce a very recognizable buzzing sound due to its electric propellers. Therefore, and as demonstrated up to 800 meters in [46], it is possible to use acoustic sensors to detect and track these types of UAVs. In this paper, a single tetrahedric array of 4 sensors was used. By using this array instead of a single detector, coherent beamforming techniques were used to increase the aperture (see Eq. 13) and to considerably improve resolution, even with the kHz wave frequency. It was comparable to a GPS tracker within a 10°accuracy. Authors of [47] proposes a more complex set-up using an "acoustic camera" comprised of a sphere of 120 sensors. The given angular resolution is 0.5°, and maximum range in a urban environment is given at around 300 m for the DJI Phantom 2. Reliability of the detection can be improved by using a data bank of known signatures.

The main drawback of the system, as discussed in both articles, is the surrounding noise. Whereas it comes from busy roads or helicopters, it can sink signal into noise, even with the use of dedicated bandpass filters [46]. Nevertheless, it is a purely passive solution, using relatively cheap components, and which can be operated at night. Using the coherence properties of sound wave, a multistatic acoustic receiver could potentially increase both range and angular precision, and could be an option for site surveillance.

3.1.3 Passive imagery

Camera and image processing are a natural solution for UAVs detection and tracking, as they are used in most generic surveillance systems. Algorithms can use either, or both, features characteristics and motion [48]. Apart from stereoscopic, multistatic systems using multiple cameras, the data produced is only 2D, and therefore there is no access to range. As mentioned with flash LiDAR, the compromise between scene resolution and FoV coverage is set by the matrix size, number of elements and the optics focal length. To better the system, multiple cameras with multiple FoV can be employed. The first, wider FoV camera can be for instance dedicated to rough detection of potential objects, which can be refined with the smaller FoV, higher resolution camera. Of course, such a set-up would require mobile elements such as point-tilt systems, which can heavily increase the total price.

Camera are very widespread, and therefore relatively cheap. Image processing algorithms for detection, recognition and tracking are also been developed for decades, therefore the field is mature. Another advantage is the high precision of camera compared to RF-based system, as it relies on light wave with a lower diffraction limit. The main drawback of passive imagery is poor performances in lower visibility scenario such as foggy, rainy, clouding weather and during the night. Using infrared camera help with penetration through obscurants [49], but resolution is limited and price is usually high. Non line-of-sight imaging is also a challenge in most urban environment.

3.2 Active LiDAR

As seen previously, no stand-alone solution seems ideal to detect and track UAV. Each have its own advantages and drawbacks. To improve global performances, LiDAR was therefore tested as a complementary sensor. Compared to passive imagery, the system works in degraded weather or during the night, and produces range information. Because it is an active system, signal to noise ratio is expected to be better than for passive systems such as RF and acoustic sensors, while being more resolved due to optical wavelength. Resolution will be better compared to radar, but non-line of sight imaging is not possible, and bad weather scene penetration is lower. Moreover, laser based systems must be limited in power due to eye-safety regulation, therefore a long range system may not be suitable in populated areas.

We describe here two types or LiDAR used for this specific application. One use gated imagery, and the other a scanning mechanism.

3.2.1 Flash, gated imager

Flash, gated imagers usually operate in the IR region. For eye-safety consideration, the wavelength of predilection is often in the SWIR, close to 1500 nm to maximize usable peak power. Flash imagers are made with a 2D matrix detector (camera), which is electronically gated to detect light only during the specified time gate. Used with a flash laser, it is possible to acquire a range slice of a few tens of meters wide. More details on the design can be found in the previous section. Apart for signal to noise ratio and night operation, another interesting aspect of gated imaging is the ability to suppress background and foreground, making image processing algorithms more robust compared to complete 2D images [50].

As an example, we can cite here a cryocooled, 640x512 pixels, 15 μm pitch gated HgCdTe APD camera to identify diverse targets [51]. The camera FoV is 0.9°x0.7°and is able to resolve a 2.5 cm object at 1 km. The flash system is mounted on a motorized tripod and is the zoom relay option of a wider FoV (6°x5°), MWIR passive camera. With this type of resolution, long range drone recognition is possible. Nevertheless, tracking quality will heavily depends on the mechanical response of the tripod, as the camera FoV is very narrow and must be constantly tilted to follow the drone trajectory. A similar demonstrator can be cited here, specifically dedicated to drone detection and tracking [52]. The authors used an InGaAs camera of 640x480 pixels, with a FoV of 0.9°x1.2°, mounted on a pan and tilt device. The measurements show tracking improvements over conventional camera while the drone was flying in front of a forest, because the background disappear with gated imaging. Kilometric range was also disclosed with this system.

At last, the authors of [53] used a 32x32, silicium based SPAD array in a LiDAR system, light sensitive from a wavelenght of 0.3 to 0.9 μm. On the same optical axis, the SPAD array was coupled to a passive thermal camera sensitive from 8 to 12 μm. The thermal camera is used for detection of object of interest in a relatively large FoV, then transitioning to LiDAR for a higher resolution depth map. The optronics head is mounted on a gimbal turret. Depth resolution was tested at 50 cm, with a small LiDAR FoV of 0.1°and a 100 Hz refresh rate. Detection of a fixed-wing UAV was performed at 1.5 km. Other images were acquired with a LiDAR operating in the SWIR for eye-safety considerations.

3.2.2 Scanning LiDAR

Conversely, scanning LiDAR systems are less employed for drone and UAV detection. The main advantage of scanning LiDAR is the considerably wider addressable FoV compared to flash imager, at the expanse of acquisition time if image resolution is kept equal. Therefore at first glance, the system does not seem to be adapted to the detection of agile and small targets. But prototypes and commercial systems are developed to challenge this idea. All systems described here are pulsed ToF based.

The OPAL product from Neptec was tested and shown to be able to detect a drone up to 600 m[54]. The design is based on rotating prisms, and was able to achieve detection while scanning 30°of FoV at a refresh rate lower than 1 Hz. The pattern drawn is a rose with an uneven laser point density across the scene. Detection was performed when at least two echoes were found originating from the same localization, as a mean to filter false alarms. Another demonstrator developed by Hanwah systems aims to reach the 2 km range. They propose a scanning LiDAR system

able to cover a FoV of 350°x120°while able to focus on a FoV of 0.5°to increase resolution [37]. The system is based on 1 kHz bandwidth galvanometer mirrors, and mounted on a gimbal to reach this wide FoV. Resolution is very high, reaching 0.003°x0.025°. Data processing is more intensive than with the Neptec demonstration and is based on neighbor clustering to segment the scene and track the target among the noise [55].

At last, another approach is to use commercial scanning systems targeted toward automotive industry. One team used Velodyne 360°rotating scanning LiDAR with both 64 and 16 lines mounted on a vehicle to detect and track an UAV [56]. Detection range is very limited with this set-up, only up to 50 m. Vertical resolution of is 0.4 °, while horizontal resolution is 0.17°for the 64 lines, and 2°for the 16 lines. Due to the low resolution, even at this close range, the system has to rely on less than 10 points for clustering. Identification of the UAV was therefore challenging and false alarms were complex to sort due to the amount of other objects on the scene.

4 Modeling the number of echoes

Here, we propose a model to address a specific problem : at which range will the system return a high enough number of target echoes for a given recognition algorithm to accurately perform its task ? The model that we develop addresses the "direct" problem, meaning that with a defined set of parameters, we can find a probability of having a given number of echoes. To get reasonable accuracy without getting too deep into simulation complexity, a number of approximations were made, and are described in this section. Nevertheless, the problem is still highly multi-parametric and requires numerical computation.

The physical system that we model is a single source pulsed scanning LiDAR. The design and parameters should allow the detection of small and agile target at a kilometric range. To simplify, the target is considered the only object in the scene to image, but more complex scenes can be treated too. We kept the optical set-up relatively simple by using a single pulsed laser source and a single pixel photodetector, with threshold detection.

4.1 Static considerations

Designing a scanning LiDAR for detecting small ang agile targets is very challenging, as it should answer a lot of requirement about target size and reflectivity, range, resolution, scanning image rate, etc... All these parameters impact each other, and pushing the analysis of this multi-parameter problem is quite complex. Our approach here is to work from the static power budget, which is the laser power sent out of the system against the power getting back on the photodetector. We will then include dynamic configurations by working on the scanning pattern.

In our system, the detector instantaneous FoV is matched to the laser beam divergence. Therefore, at a fixed range R, the link budget can be written as

$$P_r = P_e \mathcal{G}(\alpha_i) \eta_e \eta_r \mathcal{R}_{D_r} T_a^2 \tag{15}$$

with P_e the laser peak power, η_e and η_r the emission and reception transmission efficiency, T_a the one-way atmospheric transmission coefficient, $\mathcal{R}_{D_r}$ the target reflectivity toward the system aperture of diameter D_r, and $\mathcal{G}$ the surface covering coefficient between the laser beam and the target. $\mathcal{G}$ decreases as α_i, the planar distance between the beam and the target center, increases, and is dependent on both the target and the beam profile. $\mathcal{G}$ is in practice the convolution between the beam and the object surface. We can explicit α_i as

$$\alpha_i = \sqrt{(\theta - \theta_i)^2 + (\phi - \phi_i)^2}\,, \tag{16}$$

with (θ, ϕ) the target center localization, and (θ_i, ϕ_i) the beam center localization. The i indexation will be used in the next section to address multiples beams.

Expressing the link budget in the form of Eq. (15) is rarely done in literature. Usually, one can assume lambertian target reflective properties, or using the cross-section to hide the surface covering component and the reflective interaction [57]. This way, a $1/R^2$ or $1/R^4$ dependence on the signal strength with the range R appears, which is here hidden in $\mathcal{G}$ and $\mathcal{R}_{D_r}$.

The link budget predicts the average laser power getting back at the detector. Due to detector thermal noise, background light shot noise, and laser signal shot noise, the voltage level that reaches the input of the threshold comparator is a random variable. Other random components can come from atmospheric turbulence or laser speckle effects on the target, or even from the comparator behavior. By counting the number of pulses detected compared to the number of laser pulses emitted as a function of the received power P_r, the noise level σ_n and the selected threshold factor t

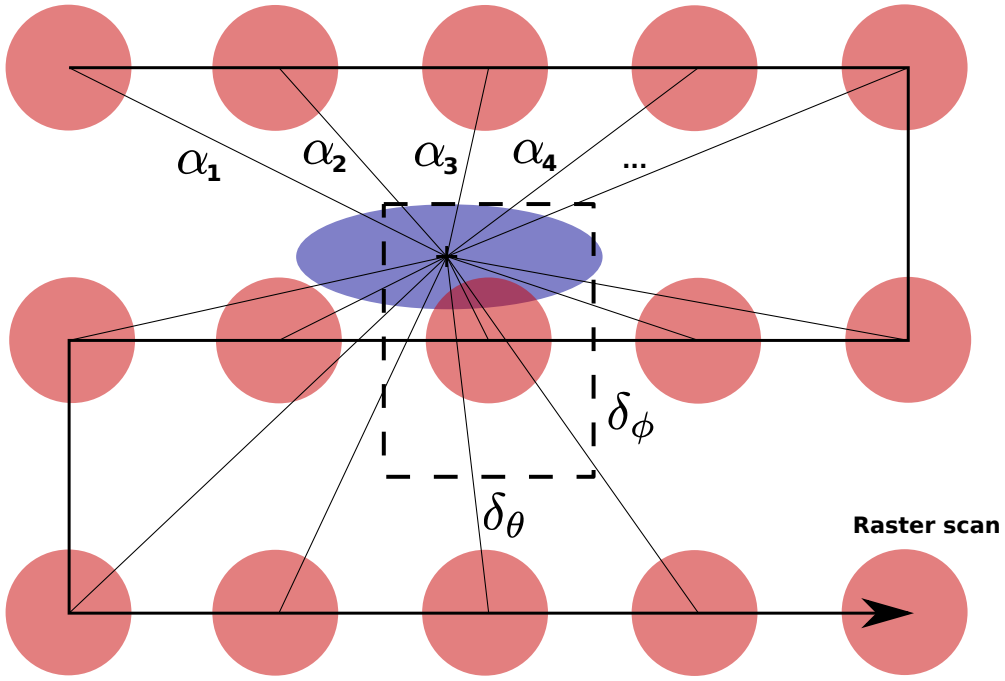

Figure 5: Illustration of a pulsed laser (red disks) raster-scan pattern with a grid parameter $(\delta_\theta, \delta_\phi)$ and an elliptic target (blue ellipse).

(detection acknowledged if $P_r \geq t\sigma_n$), we can find an expression for the probability of detection. To simplify, we suppose here that both the photo-electronic noise and the laser signal follow a Gaussian distribution of respective variance σ_n and σ_s. The resulting distribution is also Gaussian, and the pulse probability of detection $\mathcal{P}_d$ is then

$$\mathcal{P}_d = \frac{1}{2}\left(1 - \text{erf}\left(\frac{t\sigma_n - P_r}{\sqrt{2(\sigma_n^2 + \sigma_s^2)}}\right)\right) . \tag{17}$$

We now have a link between the emitted laser power, the respective target and beam position (via α_i) and profile, and the probability of detection. We then need to incorporate the scanning pattern to compute the probability of having a number of echoes on the target.

4.2 Probability of multiple echoes

The pulsed laser sequentially scans the scene with a raster-scan, producing a rectangular grid-like scan pattern. Each laser beam is separated in azimuth by δ_θ and in elevation by δ_ϕ. The target is supposed to be immobile in the scene. Because of the repetitive nature of the scan pattern, which forms kind of a lattice, we can reduce the target positions to a single mesh element Z of size $(\delta_\theta, \delta_\phi)$. For each target position (θ, ϕ) within Z, one can compute the value of $\mathcal{P}_d$ from Eq. 17 for every pulses of the raster-scan grid. Indeed, the angular distance α_i between the target center and the center of every pulse is different, leading to different $\mathcal{P}_d$. This implies that for a single target position within Z, there is potentially as much echoes as the number of pulses on the raster-scan (see Fig. 5). This computation has then to be done for all the target positions (θ, ϕ) within Z.

To better explicit our development, we can show an example of the probability to get a single echo from the pulse number i, among the total number of pulses M of the raster-scan. The pulses indexation is arbitrary, and its purpose is

only for notation. For instance, we can choose to number the pulses starting from left to right, and up to down. The probability $\mathcal{P}(N=1|i)$ to get one echo $N=1$ among the M possible echoes, from the pulse i is then

$$\mathcal{P}(N=1|i) = \frac{\iint_{\delta_\theta,\delta_\phi} \mathcal{P}_d(\theta,\phi,\theta_i,\phi_i) \prod_{j\neq i,1}^{M} \left[1-\mathcal{P}_d(\theta,\phi,\theta_j,\phi_j)\right] d\theta d\phi}{\delta_\theta \delta_\phi} . \tag{18}$$

And then the global probability to get a single echo $\mathcal{P}(N=1)$, from any of the M pulses is simply

$$\mathcal{P}(N=1) = \sum_{i=1}^{M} \mathcal{P}(N=1|i) \tag{19}$$

To simply notations, from now on, we pose $\mathcal{P}_d(l) = \mathcal{P}_d(\theta,\phi,\theta_l,\phi_l)$. To account for 2 or more echoes, the formula has to evolve drastically. Indeed, we need to take into account all the combinations for the pulses numbered (i,j) among the M possible pulses. The total number of combinations is given by $\binom{k}{M}$. To this effect, we introduce $\sigma_l^{\binom{k}{M}}$. Its expression cannot be written formally, but we can give an example for 2 echoes among 4 pulses in the following way

$$\begin{aligned}
\sigma_1^{\binom{2}{4}} =& \mathcal{P}_d(1)\mathcal{P}_d(2)(1-\mathcal{P}_d(3))(1-\mathcal{P}_d(4)) ,\\
\sigma_2^{\binom{2}{4}} =& \mathcal{P}_d(1)\mathcal{P}_d(3)(1-\mathcal{P}_d(2))(1-\mathcal{P}_d(4)) ,\\
\sigma_3^{\binom{2}{4}} =& \mathcal{P}_d(1)\mathcal{P}_d(4)(1-\mathcal{P}_d(2))(1-\mathcal{P}_d(3)) ,\\
\sigma_4^{\binom{2}{4}} =& \mathcal{P}_d(2)\mathcal{P}_d(3)(1-\mathcal{P}_d(1))(1-\mathcal{P}_d(4)) ,\\
\sigma_5^{\binom{2}{4}} =& \mathcal{P}_d(2)\mathcal{P}_d(4)(1-\mathcal{P}_d(1))(1-\mathcal{P}_d(3)) ,\\
\sigma_6^{\binom{2}{4}} =& \mathcal{P}_d(3)\mathcal{P}_d(4)(1-\mathcal{P}_d(1))(1-\mathcal{P}_d(2)) ,
\end{aligned} \tag{20}$$

There are $\binom{2}{4} = 6$ required expression of $\sigma^{\binom{2}{4}}$ in this case. We can then generalize Eq. (19) and write that the probability to have k echoes among M pulses $\mathcal{P}(N=k)$ is

$$\mathcal{P}(N=k) = \frac{1}{\delta_\theta\delta_\phi} \sum_{i=1}^{\binom{k}{M}} \iint_{\delta_\theta,\delta_\phi} \sigma_i^{\binom{k}{M}}(\theta,\phi)\, d\theta d\phi . \tag{21}$$

The probability of having at least k echoes among M pulses $\mathcal{P}(N\geq k)$ can be found by the sum $\mathcal{P}(N\geq k) = \sum_{l=k}^{M} \mathcal{P}(N=k)$. The full expression is then given by

$$\mathcal{P}(N\geq k) = \frac{1}{\delta_\theta\delta_\phi} \sum_{l=k}^{M} \sum_{i=1}^{\binom{l}{M}} \iint_{\delta_\theta,\delta_\phi} \sigma_i^{\binom{l}{M}}(\theta,\phi)\, d\theta d\phi . \tag{22}$$

It is important to highlight that this expression is not a mathematical closed-form. Each expression of $\sigma^{\binom{l}{M}}$ must be calculated by an iterative algorithm. The number of elements to sum and the complexity of the algorithm is, from the formula, at best $2^M - 1$. Therefore, increasing the number of echoes will increase computation time in an exponential manner.

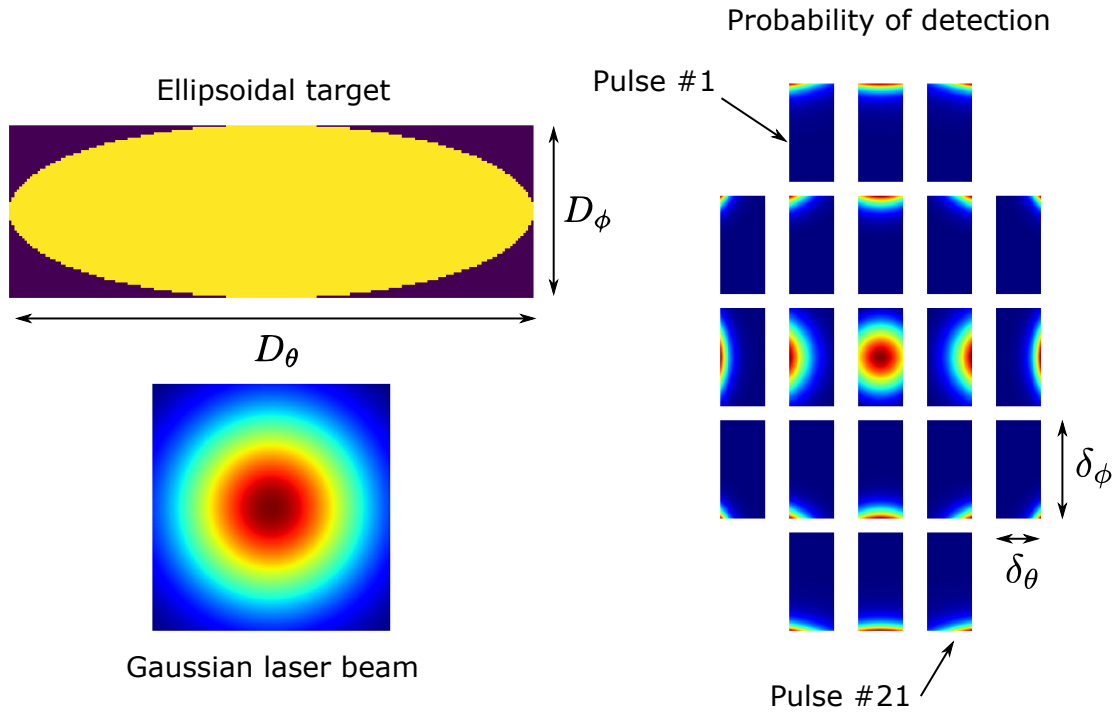

Figure 6: Illustration of a 21 laser pulses mesh used to compute the probability of echoes. On the right is shown $\mathcal{P}_d(\theta, \phi, \theta_i, \phi_i)$ for each target position (θ, ϕ) within Z, and for every one of the 21 laser pulses considered. Each element is shown at their respective pulse position to ease comprehension. The target is chosen to be elliptical with dimensions $D_\phi = 3D_\theta$. The raster scan has a dimension $\delta_\phi = 2\delta_\theta$. Dimensions and colors are not to scale between figures.

4.3 Application case

For simulation purposes, we suppose that the target is uniform, flat and has an lambertian behavior of reflectivity $\mathcal{R}_\pi$. The link budget from Eq. (15) can then be written as

$$P_r = P_e \mathcal{G}(\alpha_i) \eta_e \eta_r \mathcal{R}_\pi \left(\frac{D_r}{2R} \right)^2 T_a^2 \,. \tag{23}$$

The target is reduced to two parameters, one along the azimuth, D_θ, and one along the elevation D_ϕ. Its shape is elliptical. The laser beam intensity is supposed to be of Gaussian intensity in the plane (θ, ϕ). The beam divergence is noted Θ.

To numerically compute Eq. (22), there is a need to draw both laser beams and the target. This can be done with a 2D mesh. Then, the covering function $\mathcal{G}$ (and therefore $\mathcal{P}_d$) can be computed for every positions of the target (θ, ϕ) within Z, and for every pulses. The illustration is presented on Fig. 6.

Because we want to see the impact on range on the number of echoes, our algorithm is the following. At a range R:

1. Create a resolved enough 2D mesh for the beam and the target (cf Fig. 6). This mesh has to be re-computed for each range because of the laser beam diameter dependancy with range.
2. For each laser beams M on the raster-scan, compute on the numerical convolution $\mathcal{G}$ using its relative position to the target, for each target position within Z (illustration in Fig. 5).

Table 1: simulation parameters

Parameter	Value	Unit
P_e	2	kW
D_r	30	mm
Θ	2	mrad
$\mathcal{R}_\pi$	0.2	
η_e	1	
η_r	1	
T_a	1	
t	10	
σ_n	1	nW
σ_s	1	nW
D_θ	60	cm
D_ϕ	30	cm
δ_θ	300	μrad
δ_ϕ	500	μrad
R	300-1100	m

3. Using Eq. (23), compute P_r from the $\mathcal{G}$ mesh.
4. Using Eq. (17), compute P_d from the P_r mesh.
5. Using Eq. (22), compute $\mathcal{P}(N \geq k)$ from the P_d mesh, by summing over the mesh elements.
6. Increase the range R and go back to 1).

Because of the number of iterations needed to explore the probability of echoes dependancy along R, this method is very computation heavy. Let F be the number of ranges R considered. Then, the number of operations to perform is $F2^M$. It is exponentially increasing with the number of laser beams considered. Yet the accuracy of the model also increases with the number of echoes considered, as shown in Fig. 7, where we compare 13 beams with 21 beams. The latter computation is 256 times slower. A 3 minutes computation then becomes a 13 hours computation. The parameters used are shown in Table 1.

On Fig. 7, we can see that even if on paper system specifications can give a 90% probability of detecting a 60x30 cm target at 900 m, it is only a single point, which may not be sufficient for classifying the target. To get at least 10 echoes with a 90% probability, allowing for recognition, the target must not be farther away than 750 m, dropping 150 m to the detection limits. It should be noted that this set of parameters is only one example. It should be modified to account for every system and target specificity.

At last, increasing the resolution by lower the values of $(\delta_\theta, \delta_\phi)$ will improve the system performances in terms of range and echoes, but it will also increase the time taken to scan the scene. Therefore, there should be a compromise to be made between scan rate and resolution.

5 Conclusion

Here we gave an overview of the working principles of LiDAR systems, oriented toward the detection and tracking of small and agile targets. The main systems are based on either scanned or staring array architectures, or a mix. Range extraction can be done using amplitude, pulse, or frequency modulations. Each technique has its own advantages and drawbacks, adding either design complexity, component availability and SWAP (size, weight and power) constraints.

To detect and track targets such as drones, pluri-sensor systems have been demonstrated. They are mainly based on passive camera, acoustic sensors, passive radio-frequency, and active radar. A few studies has been done with LiDAR. Here we propose a model and a strategy to design a single emitter scanning LiDAR able to reach its required performances in term of resolution and detection range. This model can be applied to get a needed number of echoes on a specific target at a specific range. Having a high number of echoes, meaning high resolution, is the most important quality to accurately cluster and classify the point cloud. It should therefore be a very valuable design tool. Once classified, targets of interests such as UAVs can be recognized and tracked using another layer of processing.

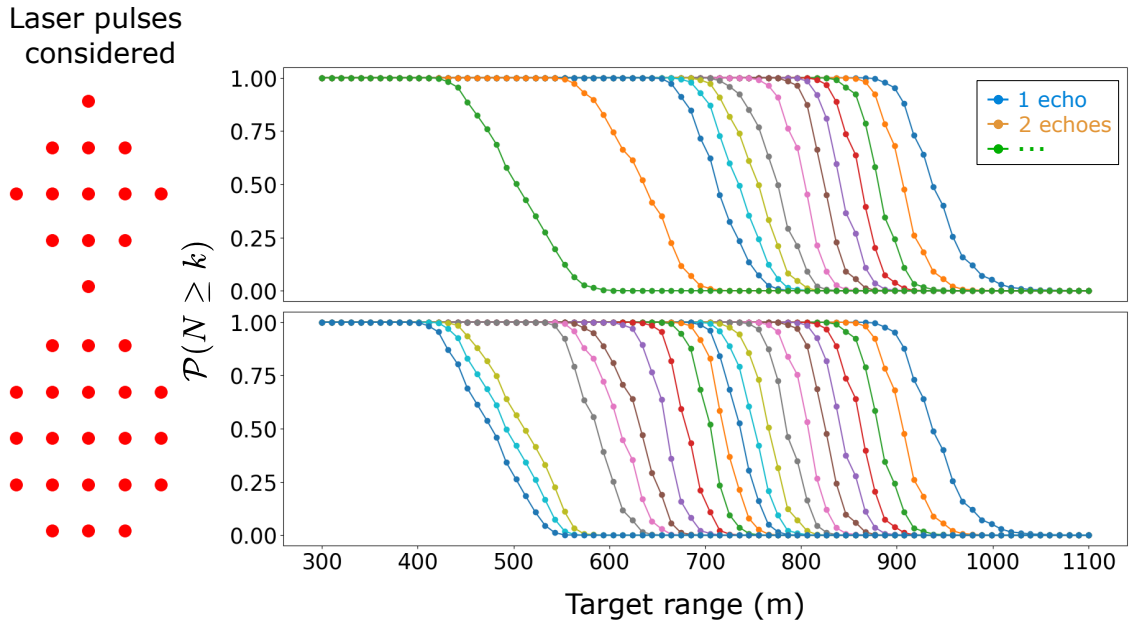

Figure 7: (Right) probability of having at least k echoes among M as a function of range, for parameters values defined in Table 1. (Left) Laser pulse arrangement considered. 13 and 21 pulses. The two resulting curves start to diverge at 8 echoes.

References

[1] G Fiocco and LD Smullin. Detection of scattering layers in the upper atmosphere (60–140 km) by optical radar. *Nature*, 199(4900):1275–1276, 1963.

[2] John M Vaughan, Kurt Ove Steinvall, Christian Werner, and Pierre Henri Flamant. Coherent laser radar in europe. *Proceedings of the IEEE*, 84(2):205–226, 1996.

[3] Jie Shan and Charles K Toth. *Topographic laser ranging and scanning: principles and processing*. CRC press, 2018.

[4] P Lutzmann, B Göhler, F Van Putten, and CA Hill. Laser vibration sensing: overview and applications. In *Electro-Optical Remote Sensing, Photonic Technologies, and Applications V*, volume 8186, page 818602. International Society for Optics and Photonics, 2011.

[5] Jeff Hecht. Lidar for self-driving cars. *Optics and Photonics News*, 29(1):26–33, 2018.

[6] Kim Hartmann and Keir Giles. Uav exploitation: A new domain for cyber power. In *2016 8th International Conference on Cyber Conflict (CyCon)*, pages 205–221. IEEE, 2016.

[7] R.D. Richmond and S.C. Cain. *Direct-detection LADAR systems*. 01 2010.

[8] Paul F McManamon. Lidar technologies and systems, 2019.

[9] Santiago Royo and Maria Ballesta-Garcia. An overview of lidar imaging systems for autonomous vehicles. *Applied Sciences*, 9(19):4093, 2019.

[10] Behnam Behroozpour, Phillip AM Sandborn, Ming C Wu, and Bernhard E Boser. Lidar system architectures and circuits. *IEEE Communications Magazine*, 55(10):135–142, 2017.

[11] PF McManamon. Design considerations for an auto lidar. In *ODS 2019: Industrial Optical Devices and Systems*, volume 11125, page 111250G. International Society for Optics and Photonics, 2019.

[12] Diego Pierrottet, Farzin Amzajerdian, Larry Petway, Bruce Barnes, George Lockard, and Manuel Rubio. Linear fmcw laser radar for precision range and vector velocity measurements. *Mrs Online Proceedings Library Archive*, 1076, 2008.

[13] Christer J Karlsson and Fredrik ÅA Olsson. Linearization of the frequency sweep of a frequency-modulated continuous-wave semiconductor laser radar and the resulting ranging performance. *Applied optics*, 38(15):3376–3386, 1999.

[14] Taehwan Kim, Pavan Bhargava, and Vladimir Stojanović. Overcoming the coherence distance barrier in long-range fmcw lidar. In *CLEO: Science and Innovations*, pages STh3L–7. Optical Society of America, 2018.

[15] S Kameyama, T Ando, K Asaka, Y Hirano, and S Wadaka. Compact all-fiber pulsed coherent doppler lidar system for wind sensing. *Applied optics*, 46(11):1953–1962, 2007.

[16] Melexis. Time-of-flight basis.

[17] John P Godbaz, Michael J Cree, and Adrian A Dorrington. Understanding and ameliorating non-linear phase and amplitude responses in amcw lidar. *Remote Sensing*, 4(1):21–42, 2012.

[18] M Chevrier and G Campanella. Lidar pulsed time of flight reference design, 2016.

[19] George M Williams. Optimization of eyesafe avalanche photodiode lidar for automobile safety and autonomous navigation systems. *Optical Engineering*, 56(3):031224, 2017.

[20] John B Mitchell, Gareth Wyn Roberts, and Paul CT Rees. Full-field, high-frequency, heterodyne interferometry for dynamic metrology based on phase detection using a modified time-of-flight camera. In *Optical Measurement Systems for Industrial Inspection XI*, volume 11056, page 110560U. International Society for Optics and Photonics, 2019.

[21] Ravil Agishev, Adolfo Comerón, Jordi Bach, Alejandro Rodriguez, Michael Sicard, Jordi Riu, and Santiago Royo. Lidar with sipm: Some capabilities and limitations in real environment. *Optics & Laser Technology*, 49:86–90, 2013.

[22] F Rutz, R Aidam, A Bächle, H Heußen, W Bronner, R Rehm, M Benecke, A Sieck, S Brunner, B Göhler, et al. Ingaas-based swir photodetectors for night vision and gated viewing. In *Electro-Optical and Infrared Systems: Technology and Applications XV*, volume 10795, page 1079503. International Society for Optics and Photonics, 2018.

[23] Long Wu, Yuan Zhao, Yong Zhang, Chenfei Jin, and Jie Wu. Multipulse gate-delayed range gating imaging lidar. *Optics letters*, 36(8):1365–1367, 2011.

[24] Martin Laurenzis and Arnaud Woiselle. Laser gated-viewing advanced range imaging methods using compressed sensing and coding of range-gates. *Optical Engineering*, 53(5):053106, 2014.

[25] Yunxiu Yang, Changdong Guo, Shijie Deng, Qian Dai, Haihua Huang, Xianguo Kou, Xiaolong Lu, Fei Yuan, Li Jing, Jianbo Gao, et al. Near-infrared array receiver for real-time 3d imaging application. In *2019 IEEE 4th Optoelectronics Global Conference (OGC)*, pages 89–93. IEEE, 2019.

[26] Masaharu Imaki, Shumpei Kameyama, Akihito Hirai, Kimio Asaka, and Yoshihito Hirano. Laser radar system, April 14 2015. US Patent 9,007,600.

[27] David S Hall. High definition lidar system, June 28 2011. US Patent 7,969,558.

[28] Angus Pacala and Mark Frichtl. Light ranging device having an electronically scanned emitter array, February 28 2019. US Patent App. 16/028,178.

[29] Xuan Truong Nguyen, Hyuk-Jae Lee, Hyun Kim, et al. A high-definition lidar system based on two-mirror deflection scanners. *IEEE Sensors Journal*, 18(2):559–568, 2017.

[30] Han Woong Yoo, Norbert Druml, David Brunner, Christian Schwarzl, Thomas Thurner, Marcus Hennecke, and Georg Schitter. Mems-based lidar for autonomous driving. *e & i Elektrotechnik und Informationstechnik*, 135(6):408–415, 2018.

[31] Seiichi Sato, Masafumi Hashimoto, Manabu Takita, Kiyokazu Takagi, and Takashi Ogawa. Multilayer lidar-based pedestrian tracking in urban environments. In *2010 IEEE Intelligent Vehicles Symposium*, pages 849–854. IEEE, 2010.

[32] Xiang Zhu. High speed 360 degree scanning lidar head, October 17 2017. US Patent 9,791,555.

[33] Louay Eldada. Three-dimensional-mapping two-dimensional-scanning lidar based on one-dimensional-steering optical phased arrays and method of using same, January 16 2018. US Patent 9,869,753.

[34] Alain Quentel, Olivier Maurice, and Xavier Savatier. Analytic model for optimizing a long-range, pulsed lidar scanner for small object detection. *Applied optics*, 58(20):5496–5505, 2019.

[35] Ismail Guvenc, Farshad Koohifar, Simran Singh, Mihail L Sichitiu, and David Matolak. Detection, tracking, and interdiction for amateur drones. *IEEE Communications Magazine*, 56(4):75–81, 2018.

[36] Xiufang Shi, Chaoqun Yang, Weige Xie, Chao Liang, Zhiguo Shi, and Jiming Chen. Anti-drone system with multiple surveillance technologies: Architecture, implementation, and challenges. *IEEE Communications Magazine*, 56(4):68–74, 2018.

[37] Byeong Hak Kim, Danish Khan, Wonju Choi, and Min Young Kim. Real-time counter-uav system for long distance small drones using double pan-tilt scan laser radar. In *Laser Radar Technology and Applications XXIV*, volume 11005, page 110050C. International Society for Optics and Photonics, 2019.

[38] Gabriel Carisle Birch, John Clark Griffin, and Matthew Kelly Erdman. Uas detection classification and neutralization: Market survey 2015. Technical report, Sandia National Lab.(SNL-NM), Albuquerque, NM (United States), 2015.

[39] Phuc Nguyen, Hoang Truong, Mahesh Ravindranathan, Anh Nguyen, Richard Han, and Tam Vu. Matthan: Drone presence detection by identifying physical signatures in the drone's rf communication. In *Proceedings of the 15th Annual International Conference on Mobile Systems, Applications, and Services*, pages 211–224. ACM, 2017.

[40] Hocheol Shin, Kibum Choi, Youngseok Park, Jaeyeong Choi, and Yongdae Kim. Security analysis of fhss-type drone controller. In *International Workshop on Information Security Applications*, pages 240–253. Springer, 2015.

[41] Michal Haluza and Jaroslav Čechák. Analysis and decoding of radio signals for remote control of drones. In *2016 New Trends in Signal Processing (NTSP)*, pages 1–5. IEEE, 2016.

[42] Folker Hoffmann, Matthew Ritchie, Francesco Fioranelli, Alexander Charlish, and Hugh Griffiths. Micro-doppler based detection and tracking of uavs with multistatic radar. In *2016 IEEE Radar Conference (RadarConf)*, pages 1–6. IEEE, 2016.

[43] M Caris, W Johannes, S Stanko, and N Pohl. Millimeter wave radar for perimeter surveillance and detection of mavs (micro aerial vehicles). In *2015 16th International Radar Symposium (IRS)*, pages 284–287. IEEE, 2015.

[44] Jan Farlik, Miroslav Kratky, Josef Casar, and Vadim Stary. Radar cross section and detection of small unmanned aerial vehicles. In *2016 17th International Conference on Mechatronics-Mechatronika (ME)*, pages 1–7. IEEE, 2016.

[45] Icnirp guidelines for limiting exposure to time-varying electric, magnetic and electromagnetic fields (up to 300 ghz), 1998.

[46] Minas Benyamin and Geoffrey H Goldman. Acoustic detection and tracking of a class i uas with a small tetrahedral microphone array. Technical report, ARMY RESEARCH LAB ADELPHI MD, 2014.

[47] Joël Busset, Florian Perrodin, Peter Wellig, Beat Ott, Kurt Heutschi, Torben Rühl, and Thomas Nussbaumer. Detection and tracking of drones using advanced acoustic cameras. In *Unmanned/Unattended Sensors and Sensor Networks XI; and Advanced Free-Space Optical Communication Techniques and Applications*, volume 9647, page 96470F. International Society for Optics and Photonics, 2015.

[48] Zhouyu Zhang, Yunfeng Cao, Meng Ding, Likui Zhuang, and Weiwen Yao. An intruder detection algorithm for vision based sense and avoid system. In *2016 International Conference on Unmanned Aircraft Systems (ICUAS)*, pages 550–556. IEEE, 2016.

[49] Byeong Kim, Min Kim, and You Chae. Background registration-based adaptive noise filtering of lwir/mwir imaging sensors for uav applications. *Sensors*, 18(1):60, 2018.

[50] Martin Laurenzis, Martin Rebert, Emmanuel Bacher, and Stéphane Schertzer. Active and passive computational imaging for tracking and prediction of three-dimensional muav flight paths. In *Electro-Optical Remote Sensing XIII*, volume 11160, page 1116009. International Society for Optics and Photonics, 2019.

[51] R Breiter, M Benecke, D Eich, H Figgemeier, T Ihle, A Sieck, A Weber, and J Wendler. Extended swir imaging for targeting and reconnaissance. In *Infrared Technology and Applications XLIV*, volume 10624, page 1062403. International Society for Optics and Photonics, 2018.

[52] Frank Christnacher, Sébastien Hengy, Martin Laurenzis, Alexis Matwyschuk, Pierre Naz, Stéphane Schertzer, and Gwenael Schmitt. Optical and acoustical uav detection. In *Electro-Optical Remote Sensing X*, volume 9988, page 99880B. International Society for Optics and Photonics, 2016.

[53] William F Woods, Dennis V Delic, Barnaby W Smith, Leszek Świerkowski, Geoffrey S Day, Vladimyros Devrelis, and Robert A Joyce. Object detection and recognition using laser radar incorporating novel spad technology. In

Laser Radar Technology and Applications XXIV, volume 11005, page 1100504. International Society for Optics and Photonics, 2019.

[54] Philip Church, Christopher Grebe, Justin Matheson, and Brett Owens. Aerial and surface security applications using lidar. In *Laser Radar Technology and Applications XXIII*, volume 10636, page 1063604. International Society for Optics and Photonics, 2018.

[55] Byeong Kim, Danish Khan, Ciril Bohak, Wonju Choi, Hyun Lee, and Min Kim. V-rbnn based small drone detection in augmented datasets for 3d ladar system. *Sensors*, 18(11):3825, 2018.

[56] Marcus Hammer, Marcus Hebel, Björn Borgmann, Martin Laurenzis, and Michael Arens. Potential of lidar sensors for the detection of uavs. In *Laser Radar Technology and Applications XXIII*, volume 10636, page 1063605. International Society for Optics and Photonics, 2018.

[57] Martin Laurenzis, Emmanuel Bacher, and Frank Christnacher. Experimental and rendering-based investigation of laser radar cross sections of small unmanned aerial vehicles. *Optical Engineering*, 56(12):124106, 2017.